Heliyon 11 (2025) e40783

Contents lists available at ScienceDirect

Heliyon

journal homepage: www.cell.com/heliyon

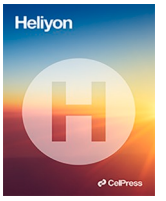

Research article

Luffa–Ni/Al layered double hydroxide bio-nanocomposite for efficient ibuprofen removal from aqueous solution: Kinetic, equilibrium, thermodynamic studies and GEP modeling

Soheil Tavassoli [a], Afsaneh Mollahosseini [a,*], Saeed Damiri [a], Mehrshad Samadi [b]

[a] Research Laboratory of Spectroscopy & Micro and Nano Extraction, Department of Chemistry, Iran University of Science and Technology (IUST), Narmak, Tehran, Iran
[b] Department of Civil and Environmental Engineering, Iran University of Science and Technology (IUST), Narmak, Tehran, Iran

ARTICLE INFO

Keywords:
Luffa
Ibuprofen
Adsorption
Layered double hydroxides
Polypyrrole
Gene expression programming

ABSTRACT

Luffa is a robust, renewable biomaterial known for its low mass, high specific strength, and non-toxicity, making it ideal for composite development. This study modified luffa to create the LF@ppy@LDH nanocomposite, combining luffa, polypyrrole, and layered double hydroxides to efficiently remove ibuprofen from water. Techniques like FE-SEM, EDX, FTIR, and XRD confirmed the modification. To optimize adsorption efficiency, factors such as contact time (*Ctime*), adsorbent dosage (*Ad*), drug concentration (*Dc*), temperature (θ), stirring rate (*Sr*), and pH were carefully fine-tuned to maximize efficiency. The highest ibuprofen removal occurred at pH 5, with an adsorption capacity of 44.306 mg/g at 298 K. The Temkin isotherm model, which points to chemisorption as the mechanism, accurately depicted the adsorption process with a high correlation coefficient ($R^2 = 0.984$). Moreover, the Elovich kinetic model proved to be the most precise in describing how ibuprofen adheres to the modified luffa, showing a very tight fit with the data ($R^2 = 0.993$). LF@ppy@LDH demonstrated outstanding reusability, maintaining steady adsorption over five repeated rounds. In addition, a powerful data-driven model, namely gene expression programming (GEP), was employed to provide an explicit formula relating input variables to removal efficiency, highlighting the potential of LF@ppy@LDH for water purification and environmental remediation.

1. Introduction

It is quite alarming how extensively pollution infiltrates different natural environments, and it continues to grow day by day. Everyday human activities, like industrial work, farming, or even waste disposal, release pollutants into our air, water, and soil, which can cause this issue [1–4]. When these pollutants find their way into places like rivers and lakes, they not only alter the water but also seriously change the living conditions for various fish and plant species [5,6]. These changes are not just temporary disruptions; they can last a long time and really damage ecosystems, which is harmful not only to wildlife but to humans as well. It is essential to find ways to confront this challenge. Actively reducing pollution can help cleanse the environment; it also helps ensure it remains healthy and sustainable for the future [7–11].

* Corresponding author.
E-mail addresses: tavassoli.soheil@gmail.com (S. Tavassoli), amollahosseini@iust.ac.ir (A. Mollahosseini), Saeeddamiri@gmail.com (S. Damiri), mehrshad1364@gmail.com (M. Samadi).

https://doi.org/10.1016/j.heliyon.2024.e40783
Received 2 August 2024; Received in revised form 8 November 2024; Accepted 27 November 2024
Available online 29 November 2024

Ibuprofen is a non-steroidal anti-inflammatory organic drug with the chemical formulation of $C_{13}H_{18}O_2$. It frequently appears in environmental studies, especially in water samples, due to its persistent nature. Traditional wastewater treatment methods often struggle to fully break down ibuprofen, leading to its accumulation in the environment. As a result, copious amounts of ibuprofen released into the environment pose a major risk to aquatic animals and even people who might drink contaminated water or eat seafood caught in these waters. In water environments, ibuprofen can interfere with the normal functions of various fish and plant species, disrupt their body systems, and alter their behavior and reproduction. For humans, there is also a concern that ibuprofen could cause stomach disorders and other health problems [12–15].

Various methods have been explored to clean up drugs like ibuprofen from water, including physical, chemical, and biological treatments. Adsorption, filtration, and membrane separation are in the physical group, while oxidation and reduction, photocatalysis, and coagulation/flocculation fall into the chemical group [16]. Biological approaches, such as biodegradation and phytoremediation, have also been mentioned for drug removal from water [17–20]. One of the most common ways to tackle this issue is through adsorption and the use of natural adsorbents like zeolites, activated carbon, and clay minerals which has gained attention as a sustainable and effective approach to eliminating drugs from water [21–23].

Layered double hydroxides (LDHs) are a type of clay-like material that have layers arranged like a sandwich, with metal hydroxide layers holding positive charges and anions sitting in between. The common expression for LDHs is $\left[M^{2+}_{1-x}\, M^{3+}_{x}\, (OH)_2\right]^{x+} [A^{n-}]_{x/n} \bullet zH_2O$, where M(II) and M(III) are divalent and trivalent metal cations, respectively, and $[A^{n-}]_{x/n}$ is an exchangeable anion. LDHs possess a high surface area, extensive pore volume, and tunable interlayer spacing, making them promising materials for various applications, including drug removal. LDHs can act as effective drug adsorbents due to their strong electrostatic interactions with charged drug molecules. The interlayer anions in LDHs can be exchanged with different species, allowing for the selective removal of specific drugs from water. Additionally, LDHs have been found to be highly stable under a wide range of environmental conditions, making them suitable for use as long-term drug removal adsorbents [24–27].

Luffa cylindrica has a fibrous morphology characterized by extensive, interconnected, and porous fibers. The fibers form a sort of network that creates a large surface area for adsorption. The fiber diameter ranges from 10 to 50 μm, and the pores usually measure between 10 and 100 μm. The fibers are composed of lignin, cellulose, and hemicellulose, which are natural polymers found on plant cell walls. Cellulose is the main component of the fibers and is responsible for their strength and rigidity, while hemicellulose and lignin provide elasticity and flexibility to the fibers. The highly porous structure of luffa cylindrica fibers allows them to absorb large amounts of water, making them ideal for water treatment applications. The fibers may undergo chemical alterations to enhance their ability to retain substances and choose specific ones. In general, the fibrous structure and chemical composition of luffa cylindrica make it a possible candidate for serving as an adsorbent in different applications, such as removing drugs from water [28–32].

Recently, there has been a significant increase in the application of data-driven models used for modeling the water treatment process [33–35]. Data-driven methods are able to discover complex relationships between variables affecting the problem and provide practical knowledge for using and estimating different parameters [36–38]. Artificial neural networks have become one of the most widely used data-driven models for modeling environmental parameters. However, one of the major disadvantages of the ANN model is that the interpretation of the results obtained from the neural network model is difficult, and they are known as black box models [39,40]. On the other hand, the gene expression programming (GEP) method is one of the white box methods that is able to provide mathematical relationships between the effective variables in the specific problem [41,42]. The GEP method is one of the powerful data-driven approaches for modeling complex processes that can provide explicit mathematical relationships for estimating the target parameter based on independent variables. In recent years, modeling adsorption processes using GEP has gained considerable attention due to their ability to establish mathematical expressions between influential parameters involved in the adsorption process. Despite its potential, limited research has been conducted on employing GEP to model the adsorption process. For example, Nguyen et al. [43] employed the GEP method to investigate cesium adsorption from aqueous solutions using Prussian blue (PB). The developed GEP model demonstrated satisfactory performance in capturing the input-output relationship for predicting adsorption behavior. Noman et al. [44] generated the mathematical prediction model for the study of antibiotic-resistant bacteria in kitchen wastewater by bimetallic bionanoparticles using GEP. Yaqub et al. [45] used GEP to evaluate and optimize the adsorption process for cesium and natural organic matter (NOM) from an aqueous solution. While GEP has demonstrated effectiveness in the adsorption process, limited studies have focused on its specific application to the adsorption process. The author's research has shown that there have been no studies in the literature exploring the use of the GEP method for removing ibuprofen from aqueous solutions. To fill this gap, we utilized the GEP method to develop a mathematical equation for the ibuprofen adsorption process. The explicit equation derived from the GEP method makes it possible to estimate the removal of ibuprofen by taking into account the key parameters involved in the adsorption process. In addition, there is no need to conduct expensive and time-consuming experimental work to determine the removal of ibuprofen under conditions similar to those obtained with the GEP-based equation.

For the first time in this study, luffa cylindrica was modified with polypyrrole and Al/Ni Layered double hydroxides to assess the removal efficiency of ibuprofen from aqueous solution. The suggested adsorbent was analyzed using field emission scanning electron microscopy, Energy Dispersive X-Ray, Fourier transform infrared, and X-ray Powder Diffraction methods, and various kinetic and isotherm models were utilized to describe the adsorption procedure. Moreover, the practical equation derived from the GEP method can estimate the removal of ibuprofen based on effective parameters.

2. Materials and methods

2.1. Experimental

2.1.1. Chemicals and equipment

The luffa employed in this study was acquired from a regional shop situated in Tehran, Iran. The metal salts, such as nickel nitrate ($Ni(NO_3)_2.6H_2O$) and aluminum nitrate ($Al(NO_3)_3.9H_2O$), were procured from Sigma and Aldrich. Pyrrole (67.09 g/mol), iron (III) chloride (162.2 g/mol), hydrochloric acid, sodium hydroxide, and methanol with 99 % purity were supplied by Merck in Germany. Urea, without any purification, was also supplied by Merck in Germany. The ibuprofen required for the experiments was obtained from Tamadkala Company located in Tehran, Iran. Deionized water was utilized in all the experiments conducted.

2.2. Instruments and measurements

To examine the morphology of LF@ppy@LDH, field emission scanning electron microscopy (SEM/EDS) was employed (Te-scan, MIRA III, Czech). Fourier transform infrared spectroscopy (FTIR) was employed to examine the chemical structure and functional groups of LF@ppy@LDH in the spectral range of 4000-400 cm^{-1}, using a Thermo AVATAR IR spectrophotometer. The physical quality of the materials was determined through powder X-ray diffraction (XRD), (Bourevestnik, DRON-8). During the adsorption analyses, the concentration of ibuprofen was determined via a UV–Vis spectrophotometer (T80+, PG, UK).

2.3. Preparation of LF@ppy@LDH

The luffa underwent a careful cleansing sequence using deionized water and ethanol to ensure the removal of any contamination or impurities. Afterward, it was dried at 313 K for a duration of 6 h. The dried luffa was then cut into small 1x1x1 centimeter pieces to be used for modification with polypyrrole.

To begin the modification process, a solution containing 0.3 M hydrochloric acid (3 mL) in 100 mL of deionized water was prepared. Subsequently, 40 mL of this HCl solution was mixed with 2 mL of pyrrole and stirred for 1 h. Following this, 1.5 g of luffa was added to another 40 mL of HCl solution and stirred accordingly. Subsequently, 6 g of iron (III) chloride were introduced to the remaining 20 mL of HCl and stirred until fully dissolved. Former studies by Yussuf et al. and Khadir et al. also employed $FeCl_3$ as the oxidant to facilitate the polymerization procedure. In the next stage, the pyrrole solution was combined with the luffa solution, and the mixture was stirred for 1 h to facilitate interaction. Subsequently, the $FeCl_3$ solution was introduced to the luffa/pyrrole blend to finalize the polymerization process. To ensure optimal polymerization, the entire solution was stirred for 24 h in an ice bath [46–48]. Upon completion of the modification, the luffa acquired a black coloration. To further refine the synthesized material, it was washed multiple times with water and methanol. In the end, the material was dried in an oven for 24 h.

0.610 g of $Al(NO_3)_3{\cdot}0.9H_2O$ and 0.928 g of $Ni(NO_3)_2{\cdot}0.6H_2O$ were dissolved in 80 mL of water using ultrasound to synthesize NiAl-LDH. Subsequently, 0.672 g of urea and LF@ppy were added to the blend. The reaction took place at 348 K for 18 h under atmospheric conditions to produce composites of NiAl-LDHs modified with luffa (LF@ppy@LDH). Afterward, the prepared LF@ppy@LDH was thoroughly washed and dried at 328 K. For comparison, the urea hydrolysis method was directly used to modify LDH on the surface of luffa (LF@LDH) as a control experiment [24]. All of the mentioned steps are illustrated in Fig. 1.

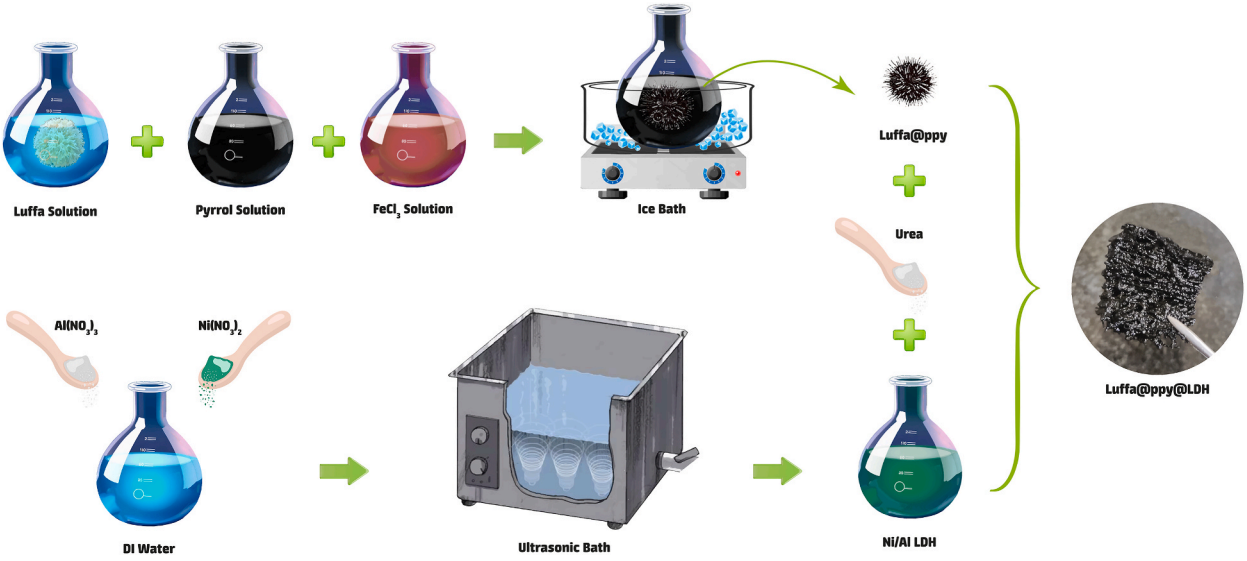

Fig. 1. The synthesis process of LF@ppy@LDH

2.4. Gene expression programming (GEP)

Gene expression programming (GEP) is introduced as a novel method for generating computer programs through the use of a genotype/phenotype genetic algorithm. The GEP algorithm is a type of evolutionary computing used to figure out complex functional relationships between input and output variables for a particular problem. The GEP algorithm begins by randomly creating an initial set of populations that are specifically designed for the problem domain. The GEP, including genetic algorithms and genetic programming, is a type of genetic algorithm that involves employing populations of individuals, selecting them based on their fitness, and introducing genetic variation utilizing genetic operators. GEP utilizes linear chromosomes consisting of ordered genes arranged in a head-and-tail structure. The objective of chromosomal selection is to codify expression trees (ETs). The algorithm achieves high efficiency by creating independent entities, namely the genome and expression tree, each with distinct functions. The common fitness functions are MAE, RRSE, and RMSE, which are problem-specific and can be determined based on the desired results [49]. The population exhibiting the highest level of precision is chosen to generate the next generation. Genetic operators, such as crossover and mutation, are applied to designated chromosomes in order to produce new offspring.

The outcomes of GEP develop several sub-expressions (sub-ETs) that can be expressed mathematically. These sub-ETs are then combined using arithmetic operators such as addition, multiplication, subtraction, and division to estimate the output parameter based on independent variables. Fig. 2 displays an illustration of simple expression trees (ETs).

The mathematical expression related to this figure can be expressed as follows:

$$\sqrt[3]{(c0 \times d1) + (c1 \times d2)}$$

2.5. Governing parameters, data samples, and performance assessment criteria

For the development of GEP, the input variables, including time (*Ctime*), stirring rate (*Sr*), *PH*, concentration of IBP (*Dc*), Adsorbent dosage (*Ad*), and temperature (θ), are used for the prediction of removal efficiency (*R*). The functional relationship between input and output variables is as follows:

$$R = f(Ctime, Ad, Dc, \theta, Sr, PH) \tag{1}$$

For evaluation of the accuracy and performance of the GEP model, three common statistical indices, such as the correlation coefficient (*CC*), root mean squared error (*RMSE*), and mean absolute error (*MAE*) were employed and defined as follows:

$$CC = \frac{\sum_{i=1}^{i=n}\left[\left(R_i^{mes} - \overline{R^{mes}}\right)\left(R_i^{\mathrm{pre}} - \overline{R^{\mathrm{pre}}}\right)\right]}{\sqrt{\sum_{i=1}^{i=n}\left(R_i^{mes} - \overline{R^{mes}}\right)^2} \cdot \sqrt{\sum_{i=1}^{i=n}\left(R_i^{\mathrm{pre}} - \overline{R^{\mathrm{pre}}}\right)^2}} \tag{2}$$

$$\mathrm{MAE} = \frac{1}{n}\sum_{i=1}^{i=n}\left|R_i^{mes} - R_i^{pre}\right| \tag{3}$$

$$RMSE = \sqrt{\frac{1}{n}\sum_{i=1}^{i=n}\left(R_i^{mes} - R_i^{pre}\right)^2} \tag{4}$$

In which *n* represents the number of measured values, R_i^{mes} and R_i^{pre} denote the ith measured and estimated R values, respectively. $\overline{R^{mes}}$ and $\overline{R^{\mathrm{pre}}}$ represent the averages of measured and predicted R values, respectively.

3. Results and discussion

3.1. Characterization

Fig. 3 illustrates the configuration and anatomy of raw luffa, and LF@ppy@LDH using SEM images. Fig. 3(a, b) displays the sponge-

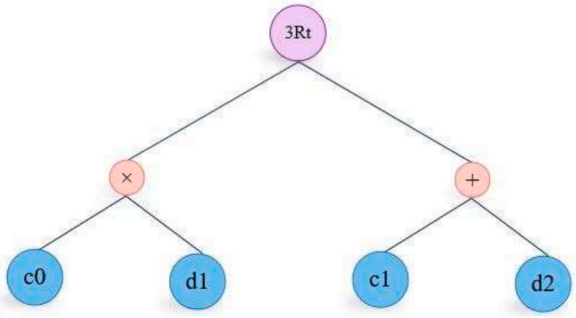

Fig. 2. Illustration of expression trees (ETs).

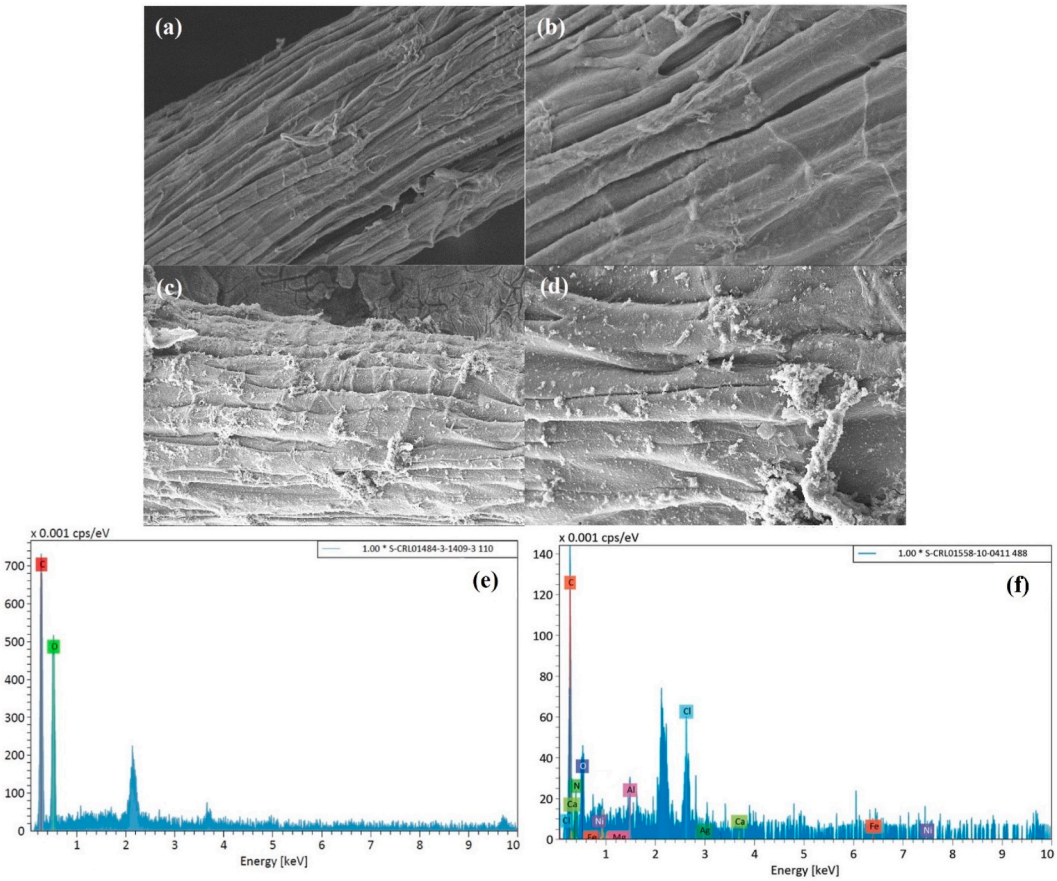

Fig. 3. SEM pictures of raw luffa (a, b), LF@ppy@LDH (c, d) and EDS investigation of raw luffa (e), and LF@ppy@LDH (f).

like structure of raw luffa with cracks and gaps. As seen in this image, raw luffa has a fibrous structure and there is a noticeable presence of minor pores on its outer surface. Fig. 3(c, d) demonstrates the final structure and morphology of luffa modified with polypyrrole and LDH crystals. As observed, some areas are covered with colonies of spherical polypyrrole particles, increasing the porosity of the absorbent and creating suitable regions for pollutant adsorption. Furthermore, LDHs form aggregates due to the stacking of individual layers and the crystals were evenly distributed on the surface, creating sufficient areas for adsorption. This

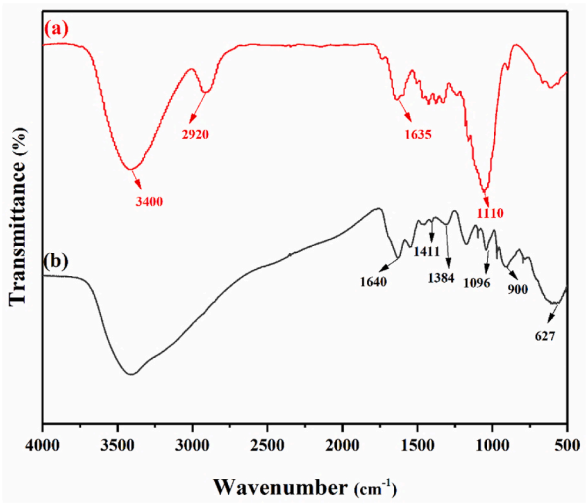

Fig. 4. FT-IR spectra of raw luffa (a), and LF@ppy@LDH (b).

suggests that the LDHs were effectively attached to the adsorbent [7].

Fig. 3(e, f) demonstrates the application of energy-dispersive X-ray (EDS) to investigate the raw luffa and LF@ppy@LDH configurations, verifying the successful modification. To ensure a consistent surface for examination and imaging, a fine coating of gold was applied to avoid surface charging. The presence of a nitrogen signal peak in the EDS spectrum of LF@ppy@LDH proves the effective alteration using polypyrrole. Additionally, the EDS spectrum of LF@ppy@LDH provides evidence of the presence of Fe and Cl, which served as the oxidant to guide the polymerization process. Furthermore, the diagram displays the existence of Ni and Al elements on the surface of the LF@ppy@LDH adsorbent.

The FT-IR spectra of raw luffa and the LF@ppy@LDH are shown in Fig. 4. In Fig. 4(a), the peak at 3400 cm^{-1} indicates the hydroxyl stretching vibrations on the surface of luffa. The peak in 2920 cm^{-1} relates to the symmetric and asymmetric stretching vibrations of CH_2 and CH_3 groups. The peak at 1635 cm^{-1} refers to C=C and C=O vibrations which are present in the aromatic ring configuration. Moreover, the peaks at 1055 cm^{-1} and 1110 cm^{-1} show the stretching vibrations of C-OR and anhydroglucose in cellulose [30,50].

In Fig. 4(b), the peaks at 3406 cm^{-1} and 883 cm^{-1} refer to the stretching and bending vibrations of N-H. Stretching vibrations need more energy, so they show up at higher wave numbers compared to bending vibrations. The peaks at 1411 cm^{-1} and 1096 cm^{-1} refer to the stretching and bending vibrations of C-N. The absorption peak at 797 cm^{-1} is related to the bending vibrations of = C-H in the polypyrrole structure. Peaks below 627 cm^{-1} are related to the stretching vibrations of M − O in the layered double hydroxide structure. The peaks at 1384 cm^{-1} and 900 cm^{-1} are attributed to C=O vibrations [51,52].

The X-ray diffraction patterns for the raw luffa and the LF@ppy@LDH are shown in Fig. 5(a) and (b), respectively. XRD evaluation is one of the most important analytical techniques used to examine the layered structure and crystallography of LDH (Layered Double Hydroxides). This analysis is also used to detect the interlayer spacing and thickness of the layers in a crystalline compound. In the XRD pattern of the LF@ppy@LDH, the main peaks of the hydrotalcite compounds, including sharp and intense peaks at low angles and relatively weaker and asymmetrical peaks at higher angles, are clearly visible. The symmetric peaks corresponding to the (003) and (006) planes, which appear at low angles, are stronger than the other peaks. These peaks, along with the broad and asymmetrical peaks related to the (012), (110), and (113) planes, indicate the growth of the crystal structure of the nickel nitrate/aluminum nitrate layered double hydroxides in a specific direction. Additionally, the resulting diffraction patterns were cross-referenced with JCPDS card numbers, and a close resemblance was observed with card number 22–0452.

3.2. Comparison of luffa and LF@ppy@LDH

Luffa, a budget-friendly natural sorbent, exhibits remarkable potential for pharmaceutical removal. Like other natural adsorbents, luffa exhibits a negatively charged surface, allowing it to attract positively charged compounds via electrostatic interactions. Conversely, when the target compound similarly bears a negative charge, repulsive forces inhibit adsorption. To tackle this challenge, a novel biosorbent called LF@ppy@LDH was prepared. The comparative efficacy of raw luffa and LF@ppy@LDH in removing ibuprofen is shown in Fig. 6. The results revealed that LF@ppy@LDH outperformed raw luffa by a significant margin, displaying an impressive 11-fold increase in ibuprofen removal efficiency. Hence, the synthesized LF@ppy@LDH has a high potential as an adsorbent for drug elimination.

3.3. The effect of operational factors

3.3.1. Effect of contact time

The length of time the drug and modified luffa are in contact greatly affects how well contaminants are absorbed, demonstrating

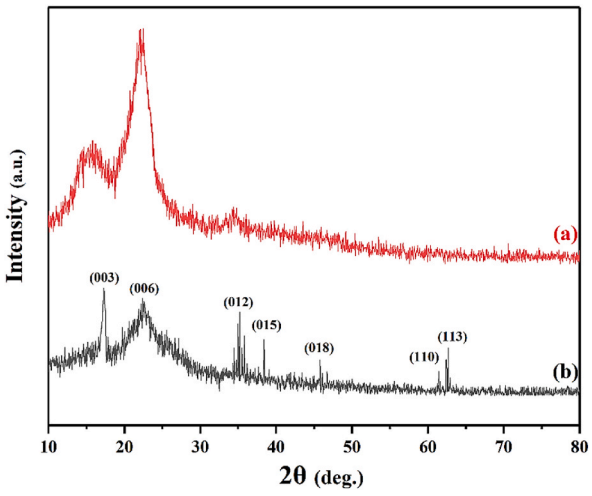

Fig. 5. XRD patterns of raw luffa (a), and LF@ppy@LDH (b).

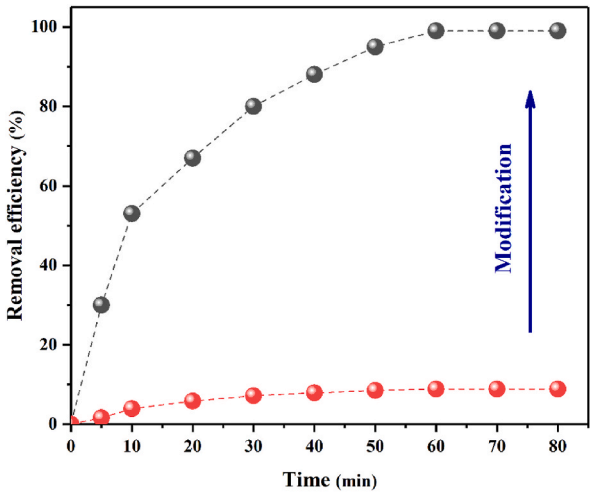

Fig. 6. Comparison of LF@ppy@LDH with raw luffa in eliminating ibuprofen.

that this method could have considerable potential for efficient ibuprofen removal. Fig. 7 offers a visual depiction of the ibuprofen removal efficiency. LF@ppy@LDH exhibits varying adsorption capacity for ibuprofen during the 0 to 80-min interval. Fig. 7 reveals that ibuprofen is absorbed at a steady rate, stabilizing after 60 min. By this point, the process successfully eliminates over 99 % of ibuprofen from the solution. In the next phase, extending from 60 to 80 min, the adsorption capacity culminates. Early on, numerous active sites are open to ibuprofen, facilitating a rapid rate of adsorption until a state of equilibrium is established. As these sites become fully saturated, they no longer accommodate further analyte molecules, signaling the conclusion of the adsorption sequence.

3.3.2. Effect of adsorbent dosage

The amount of adsorbent employed throughout the adsorption process is crucial, considering both financial and operational implications. Excessive use of adsorbents can lead to environmental degradation and necessitate costly purification efforts. Thus, determining an ideal equilibrium in the adsorbent dosage is essential to foster both effective and environmentally responsible adsorption operations. Fig. 8 illustrates the variations in ibuprofen adsorption capacity and removal efficiency observed across a spectrum of adsorbent dosages ranging from 50 to 150 mg. Elevating the adsorbent doses from 50 to 150 mg significantly enhanced the efficiency of ibuprofen removal, which escalated from 44 % to 99 %. A higher quantity of adsorbent provides additional active sites that facilitate drug removal. For the optimization of remaining parameters, an adsorbent dosage of 150 mg was selected for subsequent examinations, as it yielded optimal efficiency in drug removal.

3.3.3. Effect of drug concentration

Fig. 9 provides an evaluation of how varying initial concentrations of ibuprofen affect adsorbent efficacy. Notably, the peak removal efficiency, reaching 99 %, was observed when the ibuprofen concentration was at 100 mg/L. Conversely, the lowest removal efficiency of 67 % was detected at an ibuprofen concentration of 200 mg/L. This observation indicates that all the available active sites

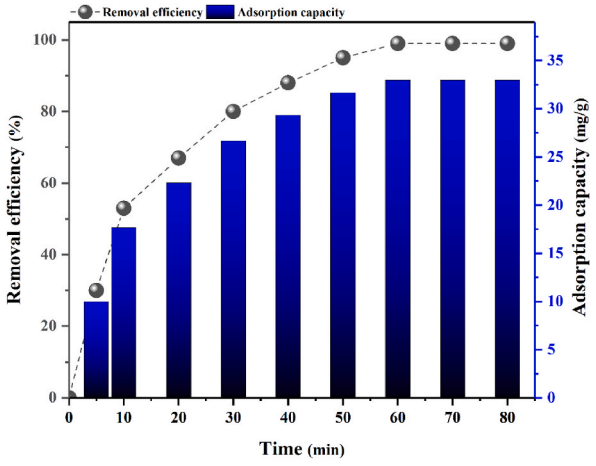

Fig. 7. The effect of contact time for ibuprofen removal by LF@ppy@LDH.

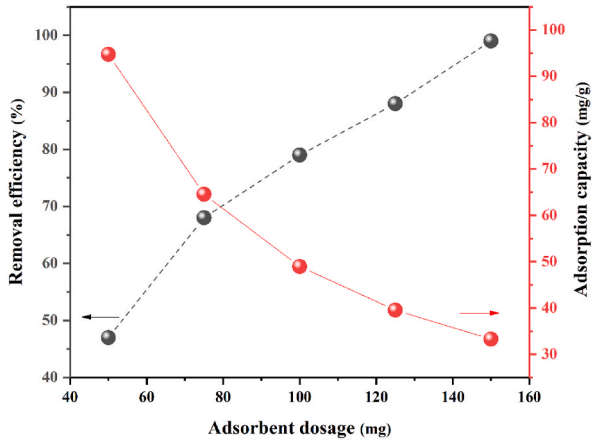

Fig. 8. The effect of adsorbent dosage for ibuprofen removal by LF@ppy@LDH.

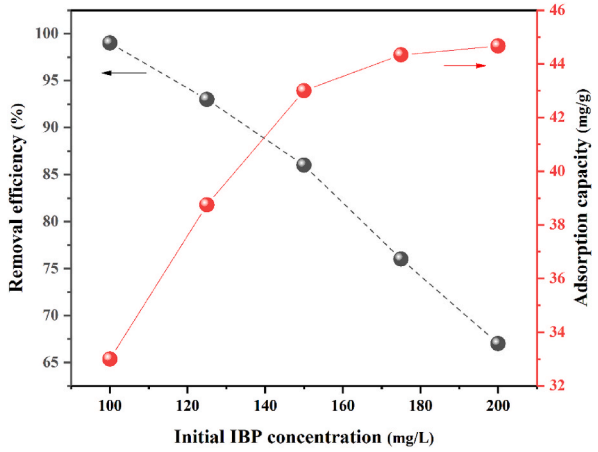

Fig. 9. The effect of ibuprofen concentration for ibuprofen removal by LF@ppy@LDH.

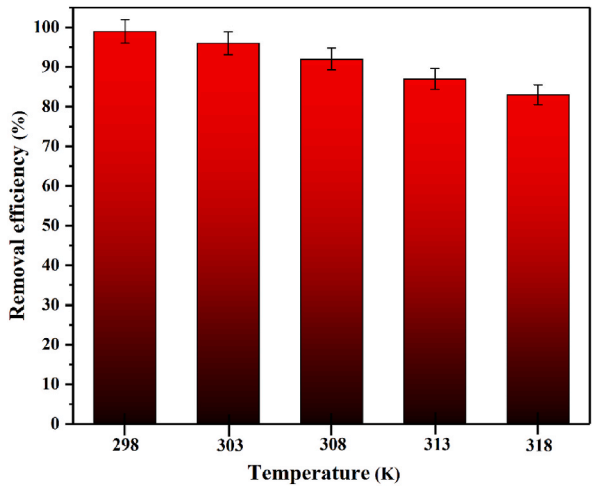

Fig. 10. The effect of temperature for ibuprofen removal by LF@ppy@LDH.

on the modified luffa were effectively utilized, and as the concentration of ibuprofen increased, the number of pollutant molecules also increased. However, at higher drug concentrations, the removal efficiency declined due to the lack of accessible and available sites. Nevertheless, nearly all the ibuprofen was effectively eliminated. The initial ibuprofen concentration of 100 mg/L was selected for subsequent examinations according to the results.

3.3.4. Effect of temperature

The effect of temperature on the efficiency of ibuprofen removal was examined by studying five distinct temperature conditions within the optimal range of 298–318 K. As shown in Fig. 10, the most favorable outcome for ibuprofen removal was observed at 298 K, which resulted in the highest adsorption efficiency. However, as the temperature increased, the efficiency of ibuprofen removal decreased, indicating an exothermic nature of the adsorption process.

3.3.5. Effect of pH

Changes in pH have a significant impact on the surface charge of the LF@ppy@LDH adsorbent and the molecular charge of ibuprofen. The influence of pH on ibuprofen removal rates was studied from 3 to 10. Fig. 11 shows that the best removal percentage of ibuprofen was detected at 5. Given that ibuprofen is a weak acid with a pK_a of 4.10, its chemical state changes with pH: it forms a cationic species at pH levels below its pK_a, a neutral species at pH equal to its pK_a, and an anionic species at pH over its pK_a. In alkaline conditions, particularly when the pH goes over 6, ibuprofen experiences deprotonation, increasing the negative charge on the adsorbent surface. This increased negativity leads to electrostatic repulsion, consequently diminishing the adsorption efficiency. Within a pH range where values exceed the pK_a but remain below 5, the adsorption capacity is amplified due to electrostatic attraction between the anionic ibuprofen molecules and the positively charged adsorbent surface. During this pH scenario, the opposing charges of the adsorbent and ibuprofen foster enhanced adsorption. Conversely, at pH values below the pK_a, adsorption is facilitated primarily through van der Waals forces or hydrogen bonding, with ibuprofen maintaining its molecular structure, thereby rendering the adsorbent surface positively charged.

3.3.6. Effect of stirring rate

Fig. 12 shows how changing the stirring speed affects how well ibuprofen is removed. To address this effect, five different speeds ranging from 0 to 200 rpm were investigated. It is evident that the ibuprofen removal rate goes up as the stirring speed increases, hitting its highest point at 100 rpm. However, upon further escalation of the speed from 100 to 200 rpm, the ibuprofen removal rate starts to drop. This suggests that at lower stirring speeds, the LF@ppy@LDH adsorbent has more opportunities to interact with ibuprofen molecules, resulting in enhanced adsorption. Conversely, at higher speeds, the interaction possibilities decrease, leading to a reduced percentage of ibuprofen removal.

3.4. Adsorption isotherms

Comprehending how ibuprofen molecules interact with the solution and LF@ppy@LDH, serving as an adsorbent, is crucial for devising an optimal adsorption approach. This paper will introduce various widely employed adsorption isotherm equations, including Temkin, Langmuir, Freundlich and Dubinin-Radushkevich, to evaluate the empirical data collected throughout the adsorption procedure [53]. Initially, the equation below presents the Langmuir isotherm in its non-linear form:

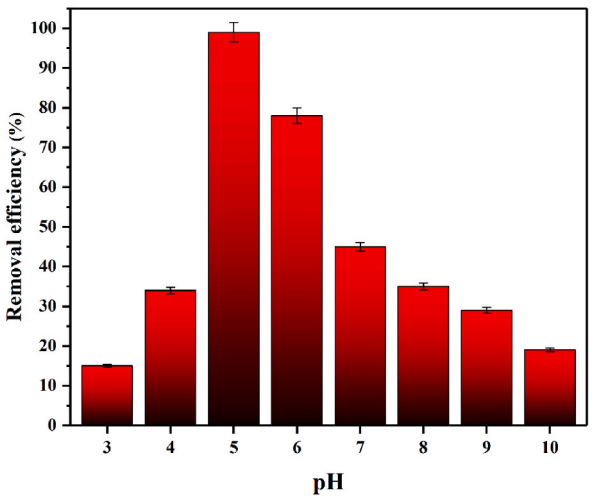

Fig. 11. The effect of pH for ibuprofen removal by LF@ppy@LDH.

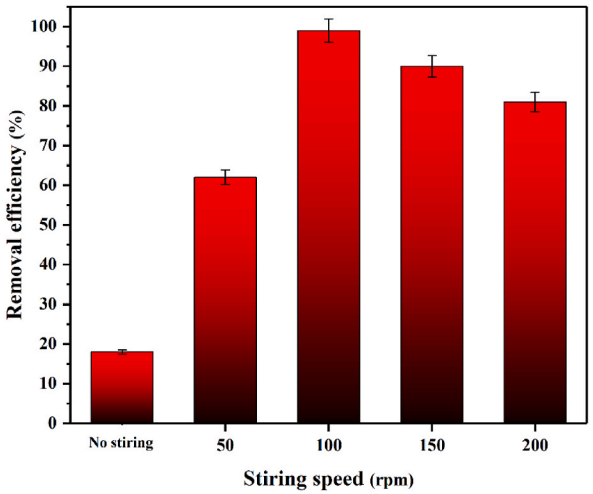

Fig. 12. The effect of stirring rate for ibuprofen removal by LF@ppy@LDH.

$$q_e = \frac{q_m K_L C_e}{1 + K_L C_e}$$

The equilibrium adsorption capacity (q_e in mg/g) and the maximum adsorption capacity (q_m in mg/g) are used in the Langmuir isotherm model. K_L (L/mg) is the model constant, and C_e (mg/L) denotes the equilibrium concentration of the drug. The fundamentals of the Langmuir isotherm can be summarized by a dimensionless equilibrium parameter (R_L) [54–56]:

$$R_L = \frac{1}{1 + K_L C_e}$$

C_0 (mg/L) represents the maximum initial concentration of the analyte, while K_L denotes the Langmuir constant. The parameter R_L indicates the extent of adsorption, which can be favorable ($0 < R_L < 1$), unfavorable ($R_L > 1$), linear ($R_L = 1$), or irreversible ($R_L = 0$). The Langmuir isotherm assumes homogeneous adsorption with a singular-layer coverage of the drug on the modified luffa surface, precluding interactions between analyte molecules. Addressing this constraint, the Freundlich isotherm emerges as a reversible framework that accommodates the heterogeneity of surfaces and transcends the limitations of solely monolayer adsorption:

$$q_e = K_f C_e^{\frac{1}{n}}$$

The equilibrium adsorption capacity is denoted by q_e (mg/g), and C_e (mg/L) is the equilibrium concentration of the drug. K_F (mg/L)

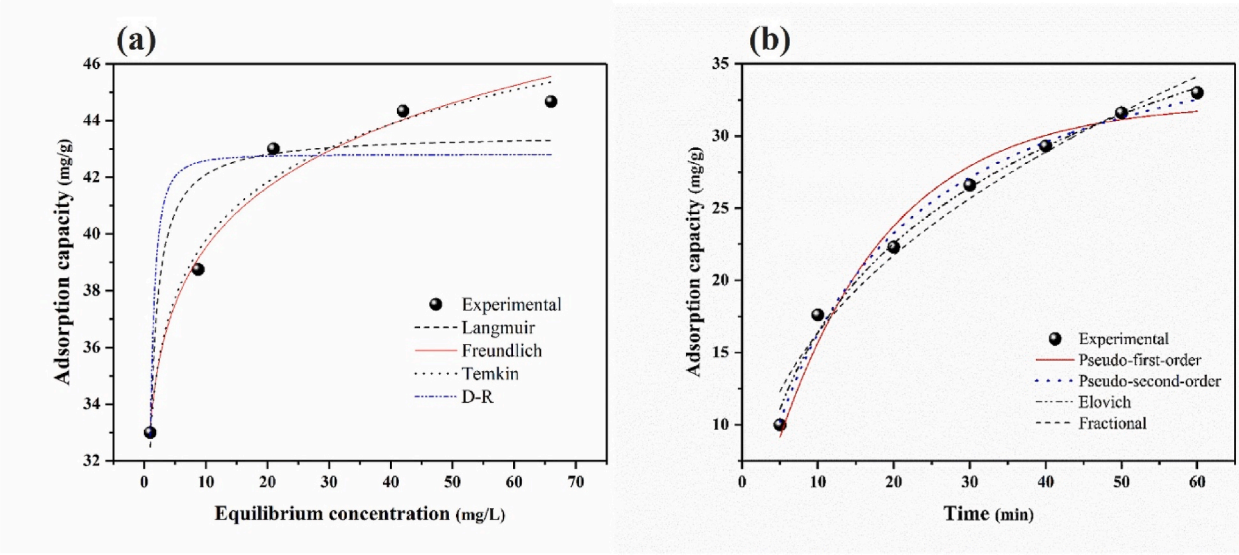

Fig. 13. (a) Isotherm fitted curves (non-linear) and (b) Kinetic plots of ibuprofen adsorption.

represents the relative adsorption capacity, while n refers to the adsorption intensity. The Temkin model defines the adsorption heat between ibuprofen and the modified luffa using the following equation [54–56]:

$$q_e = \left(\frac{RT}{b_T}\right) \ln K_T C_e$$

R stands for the universal gas constant (8.314 J/mol.K), b_T correlates with the adsorption heat constant, K_T represents the equilibrium binding constant (L/g), and T indicates the temperature (K).

The non-linear variant of the D-R isotherm is predominantly utilized for investigating the adsorption phenomena of gases or solutes on solid surfaces, particularly within the framework of porous materials. The following equation illustrates the non-linear configuration of the D-R isotherm model:

$$q_e = q_m \exp(-K\varepsilon^2)$$

$$\varepsilon = RT\ln\left(1+\frac{1}{C_e}\right)$$

$$E = \frac{1}{\sqrt{2K}}$$

q_m (mg/g) represents the maximal adsorption capacity, K (mol^2/kJ^2) denotes the isotherm constant, ε (J/mol) refers to the Polanyi potential, R stands for the universal gas constant (8.314 J/mol.K), T (K) indicates the temperature, and C_e (mg/L) signifies the equilibrium concentration of the adsorbate. The non-linear D-R isotherm is crucial for clarifying the mechanisms of adsorption and the energetic interactions in heterogeneous systems [57].

The investigation of the adsorption isotherm for ibuprofen on the modified luffa was carried out at 298 K. Numerical assessment was conducted employing the Temkin, Langmuir, Freundlich, and D-R isotherms. Fig. 13(a) displays the non-linear association between the adsorption capacity and the equilibrium concentration of ibuprofen, using an alternative approach. The Temkin isotherm exhibited superior R^2 values for ibuprofen (0.984), which aligns with the experimental adsorption data. The Temkin isotherm theory posits uniform distribution of binding energies and accounts for indirect interactions between the modified luffa and the drug. According to the Temkin isotherm, the adsorption heat decreases linearly as the surface coverage increases, indicating a chemical bonding process. A positive b_T suggests an exothermic adsorption mechanism. The R^2 values for the Freundlich and Langmuir models were also substantial but relatively smaller than the Temkin model. The R^2 value was 0.982 for the Freundlich model and 0.901 for the Langmuir model. According to the Temkin model, the n factor holds substantial significance in describing the adsorption process. The estimated value of $1/n < 1$ indicates the formation of chemical bonds on the heterogeneous surface of the modified luffa during drug removal. Therefore, the thermal uptake of the drug across the layers decreased the extent of coverage by the adsorbent nanocomposite [26,58,59]. Numerical results of isotherm models can be found in Table 1.

3.5. Adsorption kinetics

The efficiency of adsorption is primarily determined by kinetic factors, as fast kinetics are crucial in aqueous medium adsorption [20]. To assess their experimental setup, four standard kinetic models, namely pseudo-first-order (PFO), pseudo-second-order (PSO), Elovich, and fractional kinetic models, were utilized for the modified luffa. The results obtained from these kinetic models and the non-linear curve fittings are presented in Fig. 13(b) and Table 2 for ibuprofen. The pseudo-first-order kinetic model is mathematically

Table 1
Adsorption isotherm models for ibuprofen adsorption on the LF@ppy@LDH.

Isotherm models	Important parameters	Ibuprofen
Langmuir	Qmax	43.527
	KL	2.497
	R^2	0.901
	χ^2	4.467
Freundlich	Kf	33.239
	n	11.291
	R^2	0.973
	χ^2	0.844
Temkin	bT	840.352
	kT	72661.19
	R^2	0.981
	χ^2	0.677
D-R	Qm	42.812
	K	0.548
	R^2	0.792
	χ^2	6.741

Table 2
Kinetic parameters relating to the adsorption of ibuprofen on LF@ppy@LDH.

Kinetic models	Important parameters	Ibuprofen
PFO	Qe	32.309
	K1	0.058
	R^2	0.974
	χ^2	2.671
PSO	Qe	40.598
	K2	0.001
	R^2	0.991
	χ^2	0.702
Elovich	α	3.931
	β	0.094
	R^2	0.992
	χ^2	0.641
Fractional	Kp	6.393
	Vp	0.409
	R^2	0.976
	χ^2	1.963

represented as follows [54–56]:

$$q_t = q_e\left(1 - e^{-k_1 t}\right),$$

$$\ln(q_e - q_t) = \ln q_e - k_1 t$$

The following equation corresponds to the pseudo-second-order (PSO) model, which characterizes the kinetics of adsorption:

$$q_t = \frac{k_2 q_e^2 t}{1 + k_2 q_e t}$$

$$\frac{t}{q_t} = \frac{1}{k_2 q_e^2} + \frac{t}{q_e}$$

k_1 (1/min) and k_2 (g/mg.min) are the rate constants of the pseudo-first-order (PFO) and pseudo-second-order (PSO) models, respectively.

The Elovich kinetic model, which originates from the Temkin adsorption isotherm equation, is predominantly utilized to characterize the chemical adsorption of gases onto solid surfaces. The Elovich kinetic model is represented by the following equation [54–56]:

$$q_t = \frac{1}{\beta}\ln(\alpha\beta t + 1)$$

The correlation values (R^2) were compared to ascertain the most appropriate kinetic model. As shown in Table 2, the values obtained from the Elovich model (0.993) were more significant compared to the other models. Therefore, the Elovich model emerges as the most suitable framework for ibuprofen, indicating that both external mass transfer and chemisorption rate significantly influence the adsorption dynamics of the drug. Moreover, the R^2 value obtained from the Elovich model for ibuprofen was closer to one compared to those obtained from other models, demonstrating its adequacy in describing the adsorption kinetics. The parameter α functions as the desorption constant (g/mg), equivalent to the initial adsorption rate (mg/g.min), and relates to the activation energy required for chemisorption and the level of surface coverage. These findings indicate that a variety of mechanisms contribute to the adsorption of ibuprofen on modified luffa. The equation displayed below illustrates the non-linear fractional power form:

$$q_t = K_p t^{v_p}$$

The value of k_p is obtained by taking the antilogarithm of the intercept. q_t represents the amount of adsorbed analyte at time t (in minutes). V_p is a constant usually less than one when the adsorption kinetic data conforms to the power function model. As indicated in Table 2, the R^2 value for the Fractional power kinetic model was 0.977. However, in comparison to other models, the Fractional power kinetic model is not fully able to explain the experimental data adequately [7,29,60].

Table 3
Thermodynamic parameters for ibuprofen adsorption onto the LF@ppy@LDH.

ΔH° (J/mol)	ΔS° (J/mol.K)	ΔG° (J/mol)				
		298 K	303 K	308 K	313 K	318K
−109112.936	−263.545	−30576.5	−29258.8	−27941.1	−26623.4	−25305.6

3.6. Thermodynamics

Table 3 presents Van't Hoff thermodynamic details concerning ibuprofen adsorption on the modified luffa surface. These parameters (ΔG°, ΔS°, ΔH°) are used to understand the spontaneity and energy changes during the adsorption process. The following equations represent the calculation of thermodynamic values:

$$\Delta H^\circ - T\Delta S^\circ = -RTlnK_D$$

$$\Delta G^\circ = \Delta H^\circ - T\Delta S^\circ$$

$$\Delta G^\circ = -RTlnK_D$$

The gas constant R has a value of 8.314 J/(mol.K), and temperature is denoted by T in Kelvin. The distribution coefficient of adsorption is represented by K_D. To calculate the K_D value, it is necessary to know the initial concentration of the solute in the solution (C_0 before adsorption), the equilibrium concentration of the solute in the solution (C_e after adsorption), The mass of the adsorbent used (m), and the volume of the solution V. The adsorption capacity, denoted as q_e, can then be calculated using the following equation:

$$q_e = \frac{(C_0 - C_e).V}{m}$$

The distribution coefficient K_D is the ratio of the concentration of the solute in the solid phase (adsorbent) to its concentration in the liquid phase (solution) at equilibrium. It can be expressed as:

$$K_D = \frac{q_e}{C_e}$$

Where q_e is the equilibrium adsorption capacity (mg of adsorbate per gram of adsorbent), and C_e is the equilibrium concentration of the solute in the liquid phase (mg/L) [61,62].

According to Table 3, ibuprofen exhibit negative values for ΔH°, suggesting an exothermic process where lower temperatures result in greater sorption on modified luffa for ibuprofen. Enthalpy values exceeding 40 kJ/mol indicate chemisorption. In this study, the enthalpy value for ibuprofen was 109.113 kJ/mol, signifying a chemical adsorption process of drug molecules onto modified luffa. Table 3 also reveals that lower temperatures lead to more negative ΔG° values for ibuprofen, indicating a spontaneous adsorption process that becomes more feasible at low temperatures. The intercept allows for an understanding of ΔS°, and the negative values for ibuprofen indicates a decrease in system disorder, consistent with the experimental findings regarding temperature impact and the conclusions drawn from the Temkin model [26,57,63].

3.7. Adsorption mechanism

Commonly, the chief mechanisms employed for the adsorption of aquatic pollutants onto adsorbents include hydrogen bonding,

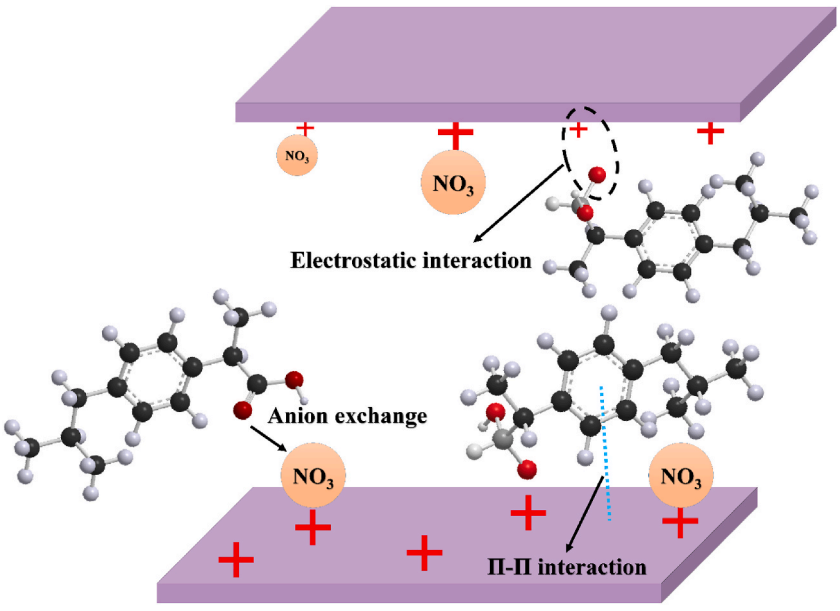

Fig. 14. The removal mechanism of ibuprofen by LF@ppy@LDH

van der Waals interactions, electrostatic force, π–π stacking, acid-base interactions, and hydrophobic interactions. However, in this study, the main motivating factor for the adsorption approach is the replacement of analyte and drug with the interlayer anion of LF@ppy@LDH, serving as the leading reason for the adsorption process. Fig. 14 illustrates the process of ibuprofen removal using the LF@ppy@LDH that was prepared. According to the explanation, the mechanism primarily involves electrostatic attraction, supported by the presence of functional groups identified through FTIR analysis, which can form bonds between the adsorbent and ibuprofen. While the experimental data supports this electrostatic interaction, additional mechanisms such as hydrogen bonding and anion exchange are also speculated to contribute to the adsorption process.

3.8. Reusability of LF@ppy@LDH

The capacity of the adsorbent to be reused is of utmost importance in both laboratory and industrial-scale adsorption experiments. This study investigated the reusability of LF@ppy@LDH under optimized circumstances, and the results are depicted in Fig. 15. Even after undergoing 5 consecutive cycles of washing with deionized water and ethanol, followed by drying at room temperature, LF@ppy@LDH retained an adsorption efficiency of 89 % for ibuprofen. These findings highlight the promising reusability potential of LF@ppy@LDH for repetitive removal of drug from aqueous solutions.

3.9. Comparison with other adsorbents

The adsorption capacity of LF@ppy@LDH adsorbent was evaluated against prior research, with the outcomes detailed in Table 4, underscoring the superior advantages of the present findings. The table shows that LF@ppy@LDH effectively eliminates ibuprofen from aqueous solution and exhibits higher adsorption capacity than what has been reported in earlier studies.

4. GEP model development

For the development of the GEP model, Equation (1) was considered for the establishment of the predictive equation for the estimation of R, incorporating six input variables. Therefore, many GEP models with different parameter settings were constructed using the trial-and-error procedure to estimate R. GEP employs arithmetic operators ($+, -, \times, \div$) and mathematical functions ($exp, sin, cos, tan, sinh, cosh, tanh, sec, log, x^2, x^3, x^4, x^5, x^{1/2}, x^{1/3}, x^{1/4}, x^{1/5}$) for generating sub-ETs. The number of genes on the chromosomes is 4. The mutation rate remained constant at 0.044. The link function type has been chosen as multiplication ($\times$). The model's training was fine-tuned to provide the best possible fit, and the root mean square error (RMSE) was used as the fitness function. Finally, the generation number was set at 1000,000. In addition, the population size and head length are selected at 30 and 8, respectively. The Sub-ETs generated by the GEP method for the prediction of R are illustrated in Fig. 16.

The relation equation for the prediction of R is as below:

$$R = Sub-ET1 \times Sub-ET2 \times Sub-ET3 \times Sub-ET4$$

$$Sub-ET1 = \sqrt[3]{\exp\left(Sin\left((c1+d1)^5 \times \sqrt[3]{d3}\right)\right)}$$

$$Sub-ET2 = Tanh\left(\exp\left(Tanh(Sec(d1)-c0) - Sin\left(\frac{d5}{c1}\right)\right)\right)$$

$$Sub-ET3 = \log\left(\left(d4^4 \times Tan(d3) - (d3 \times c0) - d4\right)^2\right)$$

$$Sub-ET4 = \mathrm{Sec}(d0) - \left(\sqrt[3]{c0 - d2 + d0 + (c1 \times c0)}\right)$$

where $d0 = Dc, d1 = PH, d2 = Sr, d3 = Ad, d4 = Ctime$ and $d5 = \theta$. The constant values in Sub-ET1 include c1 = 4.9245, in Sub-ET2 include c0 = 0.952759 and c1 = −5.265808, in Sub-ET3 include c0 = −2.173309, and in Sub-ET4 include c0 = −8.369324 and c1 = 7.963929. The scatter plots for the training and testing data are shown in Fig. 17(a) and (b), respectively. As seen, the acceptable performance of the GEP was found through scatter plots.

According to the scatter plots, the GEP models have close statistical results, and both models yielded similar results during the training and testing stages. As seen, the values of CC, RMSE, and MAE were 0.989, 4.003, and 3.014 for training and 0.986, 5.298, and 4.120 for testing data.

5. Summary and conclusions

The worldwide challenge of addressing various human disorders has made the elimination of drugs a pressing concern. To tackle this issue, this study has employed LF@ppy@LDH, which effectively removes ibuprofen, achieving impressive adsorption capacity of 44.306 mg/g. To optimize the adsorption course, identifying and controlling crucial factors, such as contact time, adsorbent dosage, drug concentration, temperature, stirring rate, and pH is important.

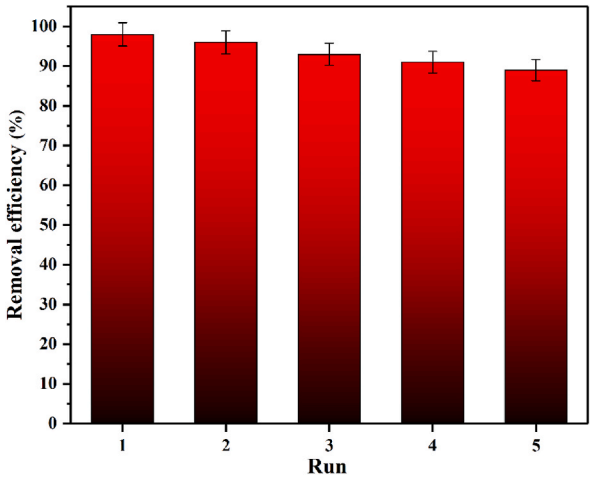

Fig. 15. Reusability of LF@ppy@LDH for ibuprofen adsorption.

Table 4
Comparison of various adsorbents for ibuprofen removal.

	Adsorbent	Adsorption capacity (mg/g)	Ref.
1	activated biochar of Aegle marmelos shell	5	[64]
2	Olive-waste cakes	10.83	[65]
3	Luffa/polypyrrole	19.16	[60]
4	Acid-modified Kola Nut Husks	24.16	[66]
5	Acid-activated bean husks	24.57	[67]
6	Cocoa-shell	23.18	[68]
7	Functionalized cocoa shell	26.98	[68]
8	AC derived from Quercus Brantii	35.49	[69]
9	cocoa shell	38.95	[70]
10	LF**@ppy@LDH**	**44.306**	This study

The findings revealed that the Temkin isotherm demonstrated the best fit for ibuprofen adsorption studies, indicating a monolayer adsorption mechanism. Additionally, the Elovich model proved to be the ideal approach for understanding the adsorption kinetics of ibuprofen.

A notable feature of the LF@ppy@LDH adsorbent is its array of exceptional benefits. It is characterized by its affordability, high efficacy in contaminant removal, and eco-friendly properties, making it a promising solution for effectively treating drug-contaminated wastewater. Furthermore, the adsorbent provides a straightforward platform for future drug removal endeavors from industrial effluent.

Looking ahead, LF@ppy@LDH holds great potential for broader applications beyond drug removal. In forthcoming investigations, it may also be employed to target diverse impurities, such as dyes and pesticides, further enhancing its versatility and impact in environmental remediation.

Finally, using the GEP method, the mathematical expression was derived for the estimation of R using effective parameters.

CRediT authorship contribution statement

Soheil Tavassoli: Writing – review & editing, Writing – original draft, Visualization, Software, Methodology, Investigation, Conceptualization. **Afsaneh Mollahosseini:** Supervision, Methodology, Conceptualization. **Saeed Damiri:** Visualization, Software, Investigation. **Mehrshad Samadi:** Writing – review & editing, Writing – original draft, Visualization, Software, Methodology, Conceptualization.

Data and code availability statement

Data will be made available on request.

Declaration of generative AI and AI-assisted technologies in the writing process

During the preparation of this work, the authors used ChatGPT to check for grammatical errors and improve the manuscript's readability. After using this tool, the authors reviewed and edited the content as needed and took full responsibility for the content of

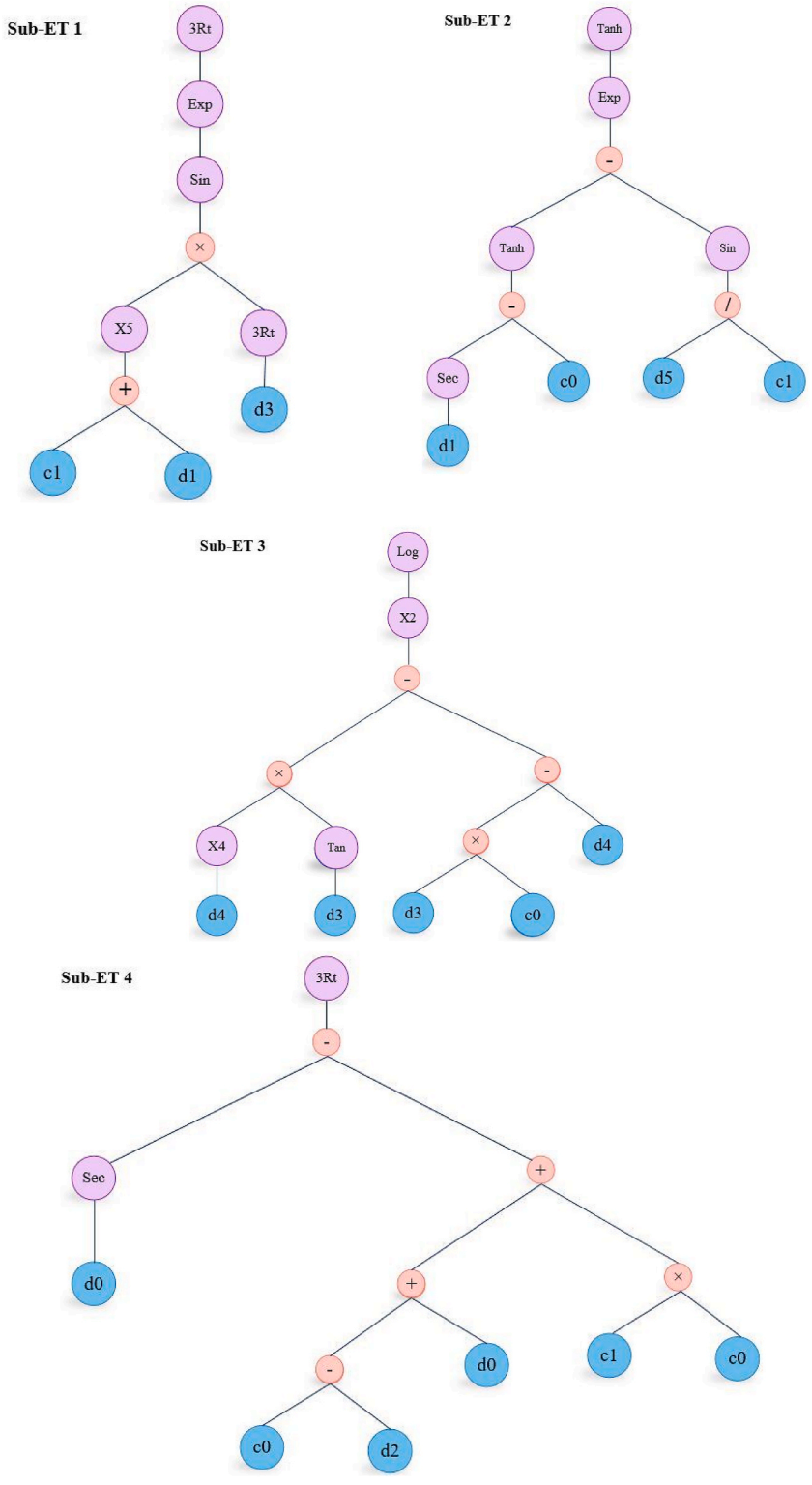

Fig. 16. Sub-expression trees from GEP for prediction of R.

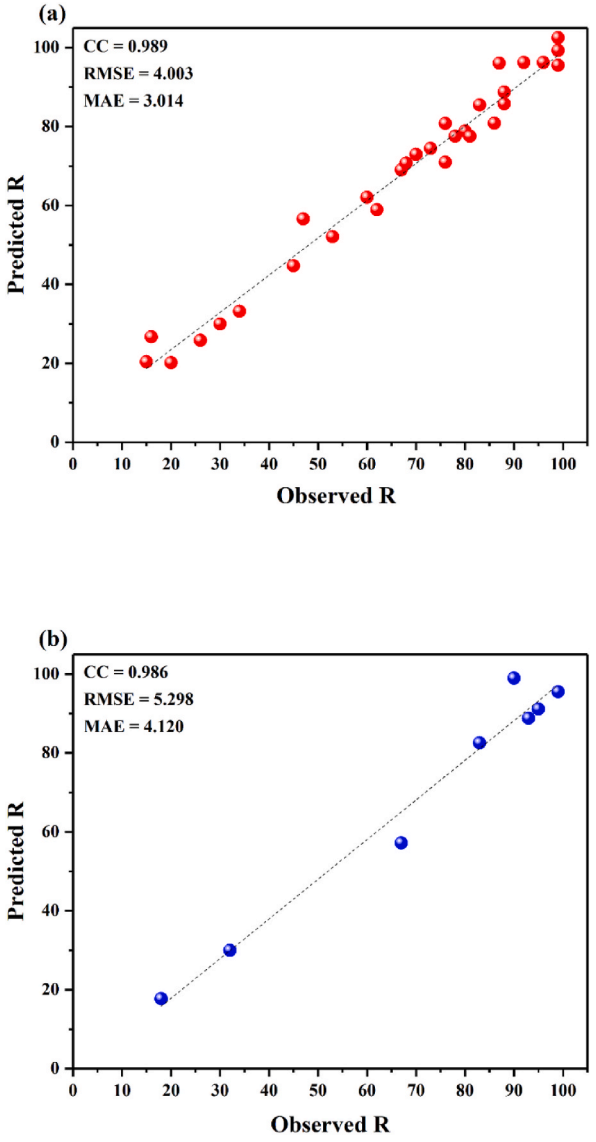

Fig. 17. The performance of GEP for prediction of R Training data (a), and Testing data (b).

the publication.

Funding

This study was not financially supported by any organizations.

Declaration of competing interest

The authors declare that they have no known competing financial interests or personal relationships that could have appeared to influence the work reported in this paper.

References

[1] A. Shahmirnoori, M. Hasani Zonoozi, M. Samadi, Evaluating groundwater quality using health risk assessment and irrigation indexes: saveh Aquifer, Iran, Water Pract. Technol. 18 (12) (Dec. 2023) 3333–3346, https://doi.org/10.2166/wpt.2023.216.
[2] I. Essamlali, H. Nhaila, M. El Khaili, Advances in machine learning and IoT for water quality monitoring: a comprehensive review, Heliyon 10 (6) (Mar. 2024) e38533055, https://doi.org/10.1016/j.heliyon.2024.e27920.

[3] M. Mao, et al., Selective capacitive recovery of rare-Earth ions from wastewater over phosphorus-modified TiO2 cathodes via an electro-adsorption process, Environ. Sci. Technol. 58 (31) (Aug. 2024) 14013–14021, https://doi.org/10.1021/acs.est.4c03241.
[4] R. Saberi, A. Nilchi, E.M. Ghasemi, A.T. Ardeshir, A. Mozaffari, Adsorption of cesium on polyaniline montmorillonite nanotube-based composite from aqueous solution, Desalination Water Treat. 166 (2019) 237–244, https://doi.org/10.5004/dwt.2019.24513.
[5] G.L. Ismaeel, et al., Fabrication and investigating of a nano-structured electrochemical sensor to measure the amount of atrazine pollution poison in water and wastewater, Chem. Data Collect. 51 (2024) 101135, https://doi.org/10.1016/j.cdc.2024.101135.
[6] N. Azhar, C.K. Yap, R. Nulit, H. Omar, W.M. Syazwan, C.S. Leow, A preliminary study of direct observation and selected water quality monitoring in Putrajaya Lake: the status between October-December 2022, Int. J. Sustain. Energy Environ. Res. 13 (1 SE-Articles) (Mar. 2024) 25–35, https://doi.org/10.18488/13.v13i1.3682.
[7] M. Negarestani, A. Mollahosseini, H. Farimaniraad, H. Ghiasinejad, H. Shayesteh, A. Kheradmand, Efficient removal of non-steroidal anti-inflammatory ibuprofen by polypyrrole-functionalized magnetic zeolite from aqueous solution: kinetic, equilibrium, and thermodynamic studies, Separ. Sci. Technol. 58 (3) (Feb. 2023) 435–453, https://doi.org/10.1080/01496395.2022.2123743.
[8] F. Mashkoor, A. Nasar, C. Jeong, Magnetized chitosan nanocomposite as an effective adsorbent for the removal of methylene blue and malachite green dyes, Biomass Convers. Biorefinery (2022) 1–13.
[9] Y. Feng, et al., Norfloxacin removal from aqueous solution using biochar derived from luffa sponge, J. Water Supply Res. Technol. 67 (8) (2018) 703–714, https://doi.org/10.2166/aqua.2018.040.
[10] I. Anastopoulos, I. Pashalidis, The application of oxidized carbon derived from Luffa cylindrica for caffeine removal. Equilibrium, thermodynamic, kinetic and mechanistic analysis, J. Mol. Liq. 296 (2019) 112078.
[11] K. Song, et al., Biosensors for detection contaminations in coffee samples: recent progress and challenges, Microchem. J. 200 (2024) 110472, https://doi.org/10.1016/j.microc.2024.110472.
[12] L.L. Mazaleuskaya, et al., PharmGKB summary: ibuprofen pathways, Pharmacogenetics Genom. 25 (2) (2015) 96.
[13] S. Chopra, D. Kumar, Ibuprofen as an emerging organic contaminant in environment, distribution and remediation, Heliyon 6 (6) (2020) e04087.
[14] M. Litynska, D. Silevych, N. Tolstopalova, I. Astrelin, Phytotoxicity of some organic pollutants, Укладач, дизайн та ѳерстка (2019) 42.
[15] M. Negarestani, et al., Preparation of sisal fiber/polyaniline/bio-surfactant rhamnolipid-layered double hydroxide nanocomposite for water decolorization: kinetic, equilibrium, and thermodynamic studies, Sci. Rep. 13 (1) (2023) 11341, https://doi.org/10.1038/s41598-023-38511-0.
[16] Z. Jiang, X. Han, C. Zhao, S. Wang, X. Tang, Recent advance in biological responsive nanomaterials for biosensing and molecular imaging application, Int. J. Mol. Sci. 23 (3) (Feb. 2022), https://doi.org/10.3390/ijms23031923.
[17] R. Davarnejad, B. Soofi, F. Farghadani, R. Behfar, Ibuprofen removal from a medicinal effluent: a review on the various techniques for medicinal effluents treatment, Environ. Technol. Innov. 11 (2018) 308–320.
[18] D.J. Lapworth, N. Baran, M.E. Stuart, R.S. Ward, Emerging organic contaminants in groundwater: a review of sources, fate and occurrence, Environ. Pollut. 163 (2012) 287–303.
[19] M. Negarestani, et al., In-situ growth of Al/Ni layered double hydroxide onto polyaniline-wrapped sisal fibers for highly efficient removal of pharmaceutical Ketoprofen and Ibuprofen contaminants: batch and fixed-bed column studies, J. Water Process Eng. 57 (2024) 104657, https://doi.org/10.1016/j.jwpe.2023.104657.
[20] S. Tavassoli, S. Cheraghi, P. Etemadifar, A. Mollahosseini, S. joodaki, N. Sedighi, Optimization and characterization of silver nanoparticle-modified luffa for the adsorption of ketoprofen and reactive yellow 15 from aqueous solutions, Sci. Rep. 14 (1) (2024) 4398, https://doi.org/10.1038/s41598-024-54790-7.
[21] F. Mohammadkhani, et al., An experimental study on absorption and catalytic activity of molybdenum-schiff bases complex immobilized on Tl2O3–SiO2 nanoparticles, Case Stud. Chem. Environ. Eng. 9 (2024) 100684, https://doi.org/10.1016/j.cscee.2024.100684.
[22] A. Mohammadkhani, F. Mohammadkhani, N. Farhadyar, M.S. Sadjadi, E. kianfar, Novel nanocomposite zinc phosphate/polyvinyl alcohol/carboxymethyl cellulose: synthesis, characterization and investigation of antibacterial and anticorrosive properties, Case Stud. Chem. Environ. Eng. 9 (2024) 100591, https://doi.org/10.1016/j.cscee.2023.100591.
[23] A. Khadir, M. Negarestani, A. kheradmand, A. Azad, M. Sillanpää, "The utilization of biomaterials for water purification: dyes, heavy metals, in: S.S. Muthu, A. Khadir (Eds.), Pharmaceuticals BT - Novel Materials for Dye-Containing Wastewater Treatment,", Springer Singapore, Singapore, 2021, pp. 27–58, https://doi.org/10.1007/978-981-16-2892-4_2.
[24] R., S. Wijitwongwan, Intasa-ard, M. Ogawa, Preparation of layered double hydroxides toward precisely designed hierarchical organization, Chem. Eng. 3 (3) (2019), https://doi.org/10.3390/chemengineering3030068.
[25] A. Kheradmand, M. Negarestani, S. Kazemi, H. Shayesteh, S. Javanshir, H. Ghiasinejad, Adsorption behavior of rhamnolipid modified magnetic Co/Al layered double hydroxide for the removal of cationic and anionic dyes, Sci. Rep. 12 (1) (2022) 14623, https://doi.org/10.1038/s41598-022-19056-0.
[26] A. kheradmand, et al., Design and preparation magnetic bio-surfactant rhamnolipid-layered double hydroxide nanocomposite as an efficient and recyclable adsorbent for the removal of Rifampin from aqueous solution, Sep. Purif. Technol. 304 (2023) 122362, https://doi.org/10.1016/j.seppur.2022.122362.
[27] A. Khadir, A. Mollahosseini, M. Negarestani, A. Mardy, in: Inamuddin, M.I. Ahamed, E. Lichtfouse, A.M. Asiri (Eds.), "Anaerobic Biotechnology for the Treatment of Pharmaceutical Compounds and Hospital Wastewaters BT - Methods for Bioremediation of Water and Wastewater Pollution,", Springer International Publishing, Cham, 2020, pp. 61–84, https://doi.org/10.1007/978-3-030-48985-4_3.
[28] A. Basem, et al., Adsorption of heavy metals from wastewater by chitosan: a review, Results Eng 23 (2024) 102404, https://doi.org/10.1016/j.rineng.2024.102404.
[29] M. Negarestani, A. Lashkari, A. Khadir, A. Mollahosseini, "Removal of rifampin by Luffa: a pharmaceutical potential in producing dye, in: S.S. Muthu, A. Khadir (Eds.), Water BT - Novel Materials for Dye-Containing Wastewater Treatment,", Springer Singapore, Singapore, 2021, pp. 209–229, https://doi.org/10.1007/978-981-16-2892-4_9.
[30] J. Arana, S. González, L. Navarrete, O. Caicedo, Luffa cylindrica as a natural adsorbent of cyanide ion in aqueous medium, Dyna 84 (201) (2017) 210–215.
[31] J.S. da Costa, A.R. Fajardo, Polypyrrole/stearic acid-coated Luffa cylindrica for enhanced removal of sodium diclofenac from water: batch and continuous adsorption studies, J. Clean. Prod. (2023) 136084.
[32] M. Negarestani, P. Etemadifar, A. Kheradmand, A Mini-Review on the Application of Magnetic-Based MOF for Dye Elimination from Polluted Waters, 2021, pp. 57–69, https://doi.org/10.1007/978-981-16-3164-1_3.
[33] H.A. Afan, et al., Data-driven water quality prediction for wastewater treatment plants, Heliyon 10 (18) (2024) e36940, https://doi.org/10.1016/j.heliyon.2024.e36940.
[34] G. Anandhi, M. Iyapparaja, Systematic approaches to machine learning models for predicting pesticide toxicity, Heliyon 10 (7) (Apr. 2024) e28752, https://doi.org/10.1016/j.heliyon.2024.e28752.
[35] A. Azma, et al., Hybrid machine learning models for prediction of daily dissolved oxygen, J. Water Process Eng. 54 (2023) 103957, https://doi.org/10.1016/j.jwpe.2023.103957.
[36] A. Azma, I. Behroyan, M. Babanezhad, Y. Liu, Fuzzy-based bee algorithm for machine learning and pattern recognition of computational data of nanofluid heat transfer, Neural Comput. Appl. 35 (27) (2023) 20087–20101, https://doi.org/10.1007/s00521-023-08851-z.
[37] A. Azma, et al., Boosting ensembles for estimation of discharge coefficient and through flow discharge in broad-crested gabion weirs, Appl. Water Sci. 13 (2) (2022) 45, https://doi.org/10.1007/s13201-022-01841-x.
[38] R. Rajab Asaad, R. Masoud Abdulhakim, The concept of data mining and knowledge extraction techniques, Qubahan Acad. J. 1 (2) (Mar. 2021) 17–20, https://doi.org/10.48161/qaj.v1n2a43. SE-Articles.
[39] M. Samadi, E. Jabbari, H.M. Azamathulla, M. Mojallal, Estimation of scour depth below free overfall spillways using multivariate adaptive regression splines and artificial neural networks, Eng. Appl. Comput. Fluid Mech. 9 (1) (Jan. 2015) 291–300, https://doi.org/10.1080/19942060.2015.1011826.
[40] M. Ghasemi, M. Samadi, E. Soleimanian, K.-W. Chau, A comparative study of black-box and white-box data-driven methods to predict landfill leachate permeability, Environ. Monit. Assess. 195 (7) (2023) 862, https://doi.org/10.1007/s10661-023-11462-9.

[41] M. Samadi, H. Sarkardeh, E. Jabbari, Explicit data-driven models for prediction of pressure fluctuations occur during turbulent flows on sloping channels, Stoch. Environ. Res. Risk Assess. 34 (5) (2020) 691–707, https://doi.org/10.1007/s00477-020-01794-0.
[42] H. Ebrahimzade, G.R. Khayati, M. Schaffie, A novel predictive model for estimation of cobalt leaching from waste Li-ion batteries: application of genetic programming for design, J. Environ. Chem. Eng. 6 (4) (2018) 3999–4007, https://doi.org/10.1016/j.jece.2018.05.045.
[43] M.N. Nguyen, M. Yaqub, S. Kim, W. Lee, Optimization of cesium adsorption by Prussian blue using experiments and gene expression modeling, J. Water Process Eng. 41 (2021) 102084, https://doi.org/10.1016/j.jwpe.2021.102084.
[44] E.A. Noman, A.A. Al-Gheethi, R.M. Radin Maya Saphira, B.A. Talip, M. Al-Sahari, N. Ismail, Mathematical prediction models for inactivation of antibiotic-resistant bacteria in kitchen wastewater by bimetallic bionanoparticles using machine learning with gene expression programming, J. Clean. Prod. 333 (2022) 130131, https://doi.org/10.1016/j.jclepro.2021.130131.
[45] M. Yaqub, M.N. Nguyen, W. Lee, Synthesis of heated aluminum oxide particles impregnated with Prussian blue for cesium and natural organic matter adsorption: experimental and machine learning modeling, Chemosphere 313 (2023) 137336, https://doi.org/10.1016/j.chemosphere.2022.137336.
[46] A. Yussuf, M. Al-Saleh, S. Al-Enezi, G. Abraham, Synthesis and characterization of conductive polypyrrole: the influence of the oxidants and monomer on the electrical, thermal, and morphological properties, Int. J. Polym. Sci. 2018 (2018).
[47] A. Khadir, M. Negarestani, H. Ghiasinejad, Low-cost sisal fibers/polypyrrole/polyaniline biosorbent for sequestration of reactive orange 5 from aqueous solutions, J. Environ. Chem. Eng. 8 (4) (2020) 103956, https://doi.org/10.1016/j.jece.2020.103956.
[48] A. Kheradmand, M. Negarestani, A. Mollahosseini, H. Shayesteh, H. Farimaniraad, Low-cost treated lignocellulosic biomass waste supported with FeCl3/Zn (NO3)2 for water decolorization, Sci. Rep. 12 (1) (2022) 16442, https://doi.org/10.1038/s41598-022-20883-4.
[49] M. Samadi, H. Sarkardeh, E. Jabbari, Prediction of the dynamic pressure distribution in hydraulic structures using soft computing methods, Soft Comput. 25 (5) (2021) 3873–3888, https://doi.org/10.1007/s00500-020-05413-6.
[50] C. Liu, C. Yan, W. Luo, X. Li, W. Ge, S. Zhou, Simple preparation and enhanced adsorption properties of loofah fiber adsorbent by ultraviolet radiation graft, Mater. Lett. 157 (2015) 303–306.
[51] F.T. Mathias, et al., Effects of low concentrations of ibuprofen on freshwater fish Rhamdia quelen, Environ. Toxicol. Pharmacol. 59 (Apr. 2018) 105–113, https://doi.org/10.1016/j.etap.2018.03.008.
[52] C. Zhong, et al., Preparation of NiAl-LDH/Polypyrrole composites for uranium (VI) extraction from simulated seawater, Colloids Surfaces A Physicochem. Eng. Asp. 562 (2019) 329–335.
[53] M. Negarestani, H. Shayesteh, A. Kheradmand, F. Pahlevani, A. Mollahosseini, S. Javanshir, Preparation of polypyrrole-functionalized recycled cotton fiber as a renewable and eco-friendly cellulose-based adsorbent for water decolorization: comprehensive batch and fixed-bed column study, Surface. Interfac. (2024) 104360, https://doi.org/10.1016/j.surfin.2024.104360.
[54] S. Mutahir, et al., Facile synthesis of Zn/Co LDH for the removal of oxytetracycline from wastewater: experimental and DFT-Based analysis, Chem. Eng. Sci. 283 (2024) 119399, https://doi.org/10.1016/j.ces.2023.119399.
[55] S. Mutahir, et al., Synthesis of mulberry wood waste biochar through acid modification for removal of dyes: experimental and DFT-based analysis, Biomass Convers. Biorefinery (2023), https://doi.org/10.1007/s13399-023-04595-x.
[56] S. Mutahir, et al., Synthesis of zeolitic imidazole framework-8 derived ZnCo layered double hydroxides for the removal of methylene blue from wastewater, Environ. Prog. Sustain. Energy 43 (1) (2024) e14228.
[57] M. Negarestani, et al., Natural and environmentally friendly rhamnolipid functionalized luffa fibers for adsorptive removal of pharmaceutical contaminant: batch and fixed-bed column studies, Chem. Eng. Sci. 299 (2024) 120552, https://doi.org/10.1016/j.ces.2024.120552.
[58] A. Khadir, M. Negarestani, A. Azad, M. Sillanpää, The utilization of biomaterials for water purification: dyes, heavy metals, and pharmaceuticals, in: Novel Materials for Dye-Containing Wastewater Treatment, Springer, 2021, pp. 27–58.
[59] G. Sriram, A. Bendre, T. Altalhi, H.Y. Jung, G. Hegde, M. Kurkuri, Surface engineering of silica based materials with Ni–Fe layered double hydroxide for the efficient removal of methyl orange: isotherms, kinetics, mechanism and high selectivity studies, Chemosphere 287 (P1) (2022) 131976, https://doi.org/10.1016/j.chemosphere.2021.131976.
[60] A. Khadir, M. Negarestani, A. Mollahosseini, Sequestration of a non-steroidal anti-inflammatory drug from aquatic media by lignocellulosic material (Luffa cylindrica) reinforced with polypyrrole: study of parameters, kinetics, and equilibrium, J. Environ. Chem. Eng. 8 (3) (2020) 103734, https://doi.org/10.1016/j.jece.2020.103734.
[61] Y. Wu, S. Fang, J. Zhang, X. Mo, L. Liu, "A review on adsorption mechanisms and distribution coefficient (kd) of cesium in clay/host rock BT, in: Proceedings of the 23rd Pacific Basin Nuclear Conference, 2023, pp. 898–912.
[62] O. Amrhar, L. El Gana, M. Mobarak, Calculation of adsorption isotherms by statistical physics models: a review, Environ. Chem. Lett. 19 (6) (2021) 4519–4547, https://doi.org/10.1007/s10311-021-01279-8.
[63] M. Motamedi, A. Mollahosseini, M. Negarestani, Ultrasonic-assisted batch operation for the adsorption of rifampin and reactive orange 5 onto engineered zeolite–polypyrrole/TiO2 nanocomposite, Int. J. Environ. Sci. Technol. 19 (8) (2022) 7547–7564, https://doi.org/10.1007/s13762-022-03951-0.
[64] P. Chakraborty, S. Banerjee, S. Kumar, S. Sadhukhan, G. Halder, Elucidation of ibuprofen uptake capability of raw and steam activated biochar of Aegle marmelos shell: isotherm, kinetics, thermodynamics and cost estimation, Process Saf. Environ. Protect. 118 (2018) 10–23, https://doi.org/10.1016/j.psep.2018.06.015.
[65] R. Baccar, M. Sarrà, J. Bouzid, M. Feki, P. Blánquez, Removal of pharmaceutical compounds by activated carbon prepared from agricultural by-product, Chem. Eng. J. 211–212 (2012) 310–317, https://doi.org/10.1016/j.cej.2012.09.099.
[66] O.S. Bello, O.C. Alao, T.C. Alagbada, O.S. Agboola, O.T. Omotoba, O.R. Abikoye, A renewable, sustainable and low-cost adsorbent for ibuprofen removal, Water Sci. Technol. 83 (1) (2021) 111–122.
[67] O.S. Bello, O.C. Alao, T.C. Alagbada, A.M. Olatunde, Biosorption of ibuprofen using functionalized bean husks, Sustain. Chem. Pharm. 13 (2019) 100151, https://doi.org/10.1016/j.scp.2019.100151.
[68] B. Jean-Rameaux, et al., Multi-functionalized cellulosic biomass by plasma-assisted bonding of α-amino carboxylic acid to enhance the removal of ibuprofen in aqueous solution, J. Polym. Environ. 29 (2021) 1176–1191.
[69] H. Nourmoradi, K.F. Moghadam, A. Jafari, B. Kamarehie, Removal of acetaminophen and ibuprofen from aqueous solutions by activated carbon derived from Quercus Brantii (Oak) acorn as a low-cost biosorbent, J. Environ. Chem. Eng. 6 (6) (2018) 6807–6815.
[70] H.A. Al-Yousef, B.M. Alotaibi, F. Aouaini, L. Sellaoui, A. Bonilla-Petriciolet, Adsorption of ibuprofen on cocoa shell biomass-based adsorbents: interpretation of the adsorption equilibrium via statistical physics theory, J. Mol. Liq. 331 (2021) 115697.